International Journal of Heat and Mass Transfer 52 (2009) 3818–3828

Contents lists available at ScienceDirect

International Journal of Heat and Mass Transfer

journal homepage: www.elsevier.com/locate/ijhmt

Buoyancy-induced flow and heat transfer in a partially divided square enclosure

Abdalla AlAmiri [a], Khalil Khanafer [b], Ioan Pop [c,*]

[a] Mechanical Engineering Department, United Arab Emirates University, United Arab Emirates
[b] Biomedical Engineering Department, University of Michigan, Ann Arbor, MI 48109, USA
[c] Faculty of Mathematics, University of Cluj, R-3400 Cluj, Romania

ARTICLE INFO

Article history:
Accepted 29 January 2009
Available online 6 April 2009

Keywords:
Cavity
Isothermal Heater
Natural convection
Numerical

ABSTRACT

The present investigation addressed buoyancy-induced heat transfer in a partially divided square enclosure. The transport equations were solved using the finite element formulation based on the Galerkin method of weighted residuals. The validity of the numerical code used was ascertained by comparing our results with previously published results. Results were obtained in terms of streamlines, isotherms, and Nusselt number for various geometrical parameters specifying the height, width and position of the heater. The effect of Rayleigh number in the range of $10^4 \leqslant Ra \leqslant 5 \times 10^7$ was highlighted in the proposed work. The results revealed that all the parameters related to the geometrical dimensions of the heater were significant on the flow field, isotherms, and heat transfer. The examined dimensionless geometric dimensions employed along with their respective ranges were: heater width ($0.005 \leqslant W \leqslant 0.5$), heater height ($0.005 \leqslant H \leqslant 0.5$), and heater location ($0 \leqslant D \leqslant 0.5$). The investigation revealed that increased heater height, width, and location has enhanced the heat transfer due to increasing the surface area of the heater.

1. Introduction

Buoyancy-induced flow and heat transfer in enclosures has received considerable attention by many researchers both experimentally and numerically (Martynenko and Khramtsov [1]). This attention stems from the importance of such geometry in cooling devices for electronic instruments, building insulations, solar collectors, double-glazed windows, and nuclear reactor core [2]. Furthermore, natural convection in a closed cavity has been used as a classical configuration for benchmark testing in CFD packages. A comprehensive survey on this subject has been presented by Ostrach [3].

Natural convection heat transfer and fluid flow in partially divided enclosures has been the subject of many studies in the last few decades because of its importance in many applications. In a number of applications related to the thermal control of electronic components [4–9], it is required to remove the generated heat from the system by maintaining the temperature of the electronic component equal or below a maximum operating temperature. This temperature plays a major role in the performance of the electronic device [10]. Different techniques have been used to obtain a well-controlled thermal environment including the traditional methods of natural and forced convective cooling. Because suitable cooling is essential yet is constrained by acoustic requirements, natural convection cooling has recently received an increasing consideration because of its quiet operation and high reliability [11].

Varol et al. [12] analyzed numerically natural convection heat transfer from a protruding heater located in a triangular enclosure. The study was formulated in terms of the vorticity-stream function procedure and numerical solution was performed using finite difference method. Their results showed that the location and height of the heater were found to significantly affect flow and temperature fields. Increased heater height was found to enhance heat transfer due to increasing heated surfaces. Yucel and Ozdem [13] studied numerically natural convection in a square enclosure with partially divided partitions using finite volume method. The horizontal end walls of the enclosure were assumed adiabatic or perfectly conducting and the vertical sides were maintained at uniform but different temperature. The results of that study demonstrated that the average Nusselt number increased with increasing Rayleigh number and decreasing the number of partitions. Dagtekin and Oztop [14] studied natural convection by two heated partitions with different heights within an enclosure. The right side wall and the bottom wall of the enclosure were insulated perfectly while the left side wall and top wall were maintained at the same uniform temperature. The partitions were placed on the bottom of the enclosure and their temperatures were kept higher than the non-isolated walls. The authors observed that the average Nusselt

* Corresponding author.
E-mail address: pop.ioan@yahoo.co.uk (I. Pop).

0017-9310/$ - see front matter © 2009 Elsevier Ltd. All rights reserved.
doi:10.1016/j.ijheatmasstransfer.2009.01.043

Nomenclature

c_p	specific heat at constant pressure
d	location of the heater
D	non-dimensional location of the heater, d/L
g	acceleration due to gravity
Gr	Grashof number, $g\beta\Delta TL^3/\nu^2$
h	height of the heater
H	non-dimensional height of the heater
k	thermal conductivity
l	length of the cavity
Nu	local Nusselt number, defined in Eq. (8)
$\bar{N}u$	average Nusselt number, defined in Eq. (9)
p	pressure
P	dimensionless pressure, $p/\rho(g\beta\Delta TL)$
Pr	Prandtl number, ν/α
Q	total heat transfer
Ra	Rayleigh number, $Gr.Pr$
T	temperature
T_C	temperature of the cold wall
T_H	temperature of the heater
u	x-velocity component
U	dimensionless x-velocity component, $u/\sqrt{g\beta\Delta TL}$
v	y-velocity component
V	dimensionless y-velocity component, $v/\sqrt{g\beta\Delta TL}$
w	width of the heater
W	dimensionless width of the heater, w/L
x	x-coordinate
X	dimensionless X-coordinate, x/L
y	y-coordinate
Y	dimensionless Y-coordinate, y/L

Greek symbols

α	thermal diffusivity
β	coefficient of thermal expansion
ν	kinematic viscosity
θ	dimensionless temperature, $(T-T_C)/(T_H-T_C)$
ρ	density

Subscripts

C	cold
H	hot
n	normal direction

number increased as the height of partitions increased and the spacing between partitions increased.

Heat transfer in a differentially heated, partitioned, square cavity containing heat generating fluid was studied numerically by Oztop and Bilgen [15]. The vertical walls and the partition attached to the bottom wall were assumed isothermal and the horizontal walls were assumed perfectly insulated. The left vertical wall was maintained at a higher temperature than both the partition and the right wall. The authors illustrated that the cold partition decreased heat transfer within the enclosure and the heat reduction was gradually increased with increasing partition height and thickness. Moreover, heat transfer within the enclosure was also found to reduce significantly when the partition was closer to the hot or cold wall. Recently, Corvaro and Paroncini [16] conducted an experimental study of natural convection in a differentially heated cavity by a hot strip through a 2D-PIV system for Rayleigh number ranged from 6.5×10^4 to 3.2×10^5. The effect of the position of the source on the fluid flow and heat transfer characteristics within the cavity was analyzed in that study.

The main objective of this investigation is to analyze laminar natural convection in a square enclosure with protruding isothermal heater. Thorough analysis of the effect of the protruding heater on the heat transfer within the cavity will be carried out for various pertinent parameters such as Rayleigh number, height of the heater, heater width, and heater location.

2. Mathematical formulation

The problem under investigation is a laminar two dimensional laminar natural heat transfer convection in a cavity with a protruding isothermal heater on the bottom wall. The physical domain under consideration and coordinate system are shown in Fig. 1. An isothermal partition of height h and width w is maintained at a temperature T_H and is placed at a distance d from the right wall as shown in the figure. The two vertical walls of the enclosure are maintained at a constant temperature T_C, while maintaining $T_H > T_C$. The horizontal walls are assumed to be insulated. In addition, the thermophysical properties of the fluid are assumed constant, except for the density in the buoyancy term in the momentum equations which is treated according to Boussinesq model.

By assimilating the above assumptions, the system of the governing equations can be expressed

2.1. Continuity equation

$$\frac{\partial U}{\partial X}+\frac{\partial V}{\partial Y}=0 \tag{1}$$

2.2. Momentum equation

$$U\frac{\partial U}{\partial X}+V\frac{\partial U}{\partial Y}=-\frac{\partial P}{\partial X}+\frac{\nabla^2 U}{\sqrt{Gr}} \tag{2}$$

$$U\frac{\partial V}{\partial X}+V\frac{\partial V}{\partial Y}=-\frac{\partial P}{\partial Y}+\frac{\nabla^2 V}{\sqrt{Gr}}+\theta \tag{3}$$

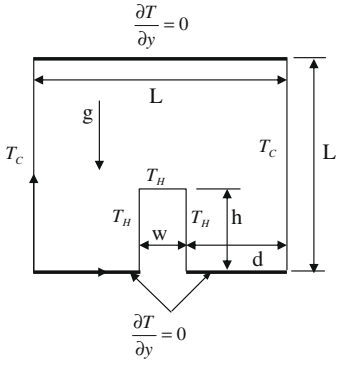

Fig. 1. Schematic for physical model.

Table 1
Comparison of the average Nusselt number between the present results and those reported in the literature.

Reference	$Ra = 10^5$	$Ra = 10^6$	$Ra = 10^8$
Present	4.522	8.826	30.23
El-Refaee et al. [23]	4.512	8.800	30.32
Barakos and Mitsoulis [2]	4.510	8.806	30.10
Markatos and Pericleous [19]	4.430	8.754	N/A
De Vahl Davis [20]	4.519	8.799	N/A
Fusegi et al. [21]	4.646	9.012	N/A
Wan et al. [22]	4.592	8.976	31.48
Henkes et al. [24]	N/A	N/A	30.4

2.3. Energy equation

$$U\frac{\partial\theta}{\partial X}+V\frac{\partial\theta}{\partial Y}=\frac{\nabla^2\theta}{Pr\sqrt{Gr}} \tag{4}$$

The above equations were normalized using the following dimensionless parameters:

$$(U,V)=\frac{(u,v)}{\sqrt{g\beta\Delta TL}},\quad P=\frac{p}{\rho(g\beta\Delta TL)},\quad \theta=\frac{T-T_C}{T_H-T_C},$$
$$(X,Y)=\frac{(x,y)}{L}, \tag{5}$$

where β is the fluid thermal expansion coefficient, ρ the fluid density, g the gravitational acceleration, P the dimensionless pressure, U and V are the velocity components in x- and y-direction, respectively. In addition, the relevant Grashof number and Prandtl number are given by $Gr = g\beta\Delta TL^3/\nu^2$ and $Pr = \nu/\alpha$, respectively.

The associated boundary conditions for the problem under consideration can be expressed as:

$$\begin{aligned} &X=0,1\ \&\ 0\leqslant Y\leqslant 1: && U=V=\theta=0\\ &Y=1\ \&\ 0\leqslant X\leqslant 1: && U=V=\tfrac{\partial\theta}{\partial Y}=0\\ &Y=0\ \&\ 0\leqslant X\leqslant (D+W),(D+W)\leqslant X\leqslant 1 && U=V=\tfrac{\partial\theta}{\partial Y}=0 \end{aligned} \tag{6}$$

On the heater wall:

$$U=V=0,\quad \theta=1 \tag{7}$$

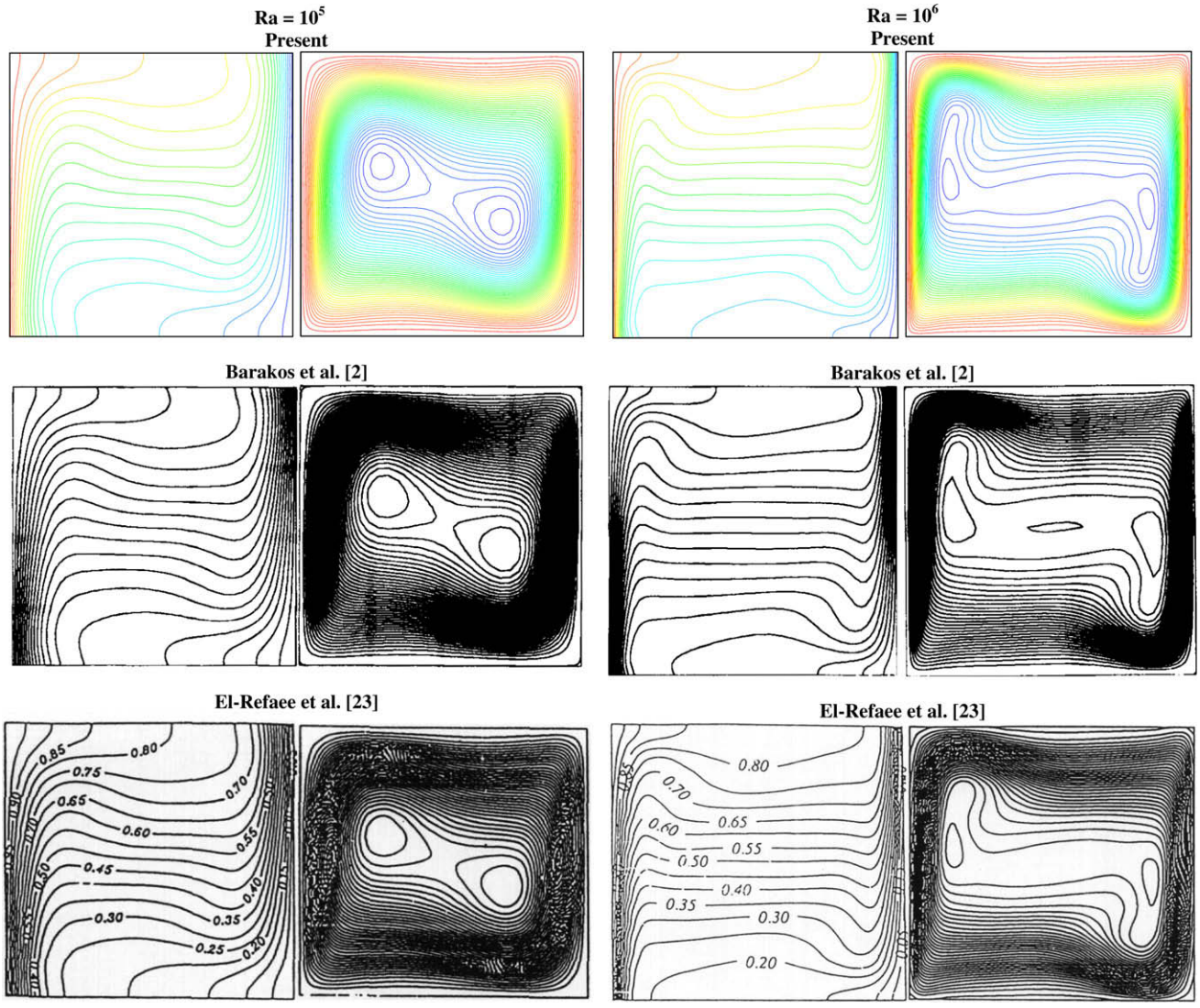

Fig. 2. Comparison of the isotherms and streamlines between the present results and other results reported in the literature at various Rayleigh numbers.

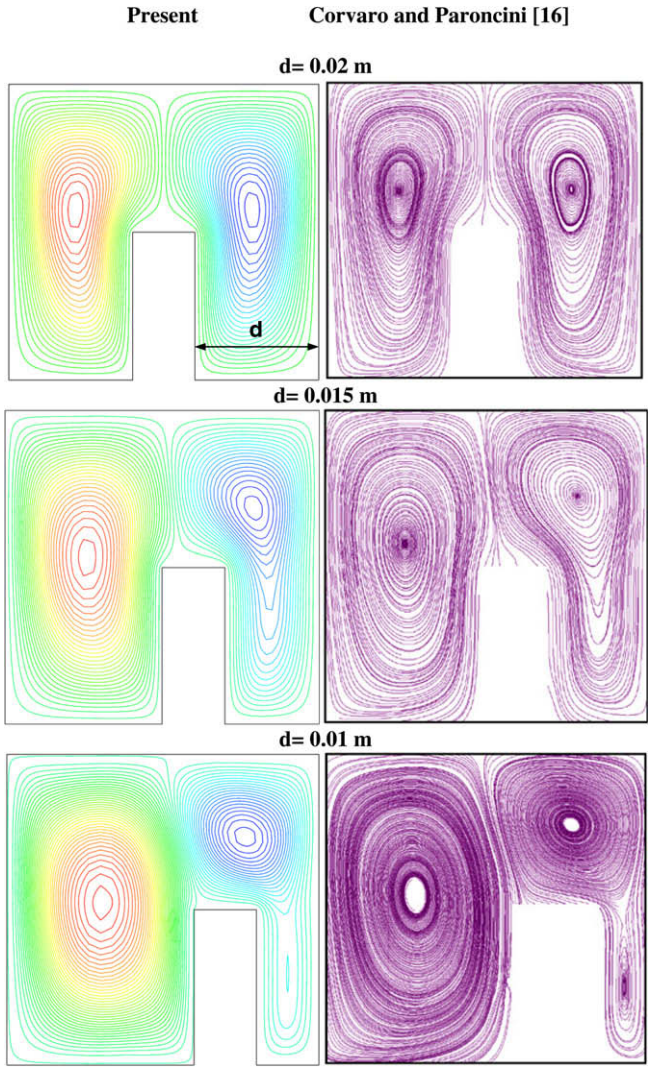

Fig. 3. Comparison of the streamlines between the present results and the PIV-experimental results of Corvaro and Paroncini [16] ($Ra = 6.39 \times 10^4$).

The local Nusselt along the vertical wall of the enclosure is defined as

$$Nu_{n,\text{left wall}} = -\left.\frac{\partial\theta}{\partial X}\right|_{X=0}, Nu_{n,\text{right wall}} = -\left.\frac{\partial\theta}{\partial X}\right|_{X=1} \tag{8}$$

Accordingly, the average Nusselt number is calculated by integrating the local Nusselt number along the wall

$$\overline{Nu} = \int_0^1 -\frac{\partial\theta}{\partial X}dY \tag{9}$$

3. Numerical scheme

A finite element formulation based on the Galerkin method was employed to solve the governing equations. The application of this technique is well documented by Taylor and Hood [17] and Gresho et al. [18]. In the current investigation, the continuum domain was divided into a set of non-overlapping regions called elements. Nine node quadrilateral elements with bi-quadratic interpolation functions were utilized to discretize the

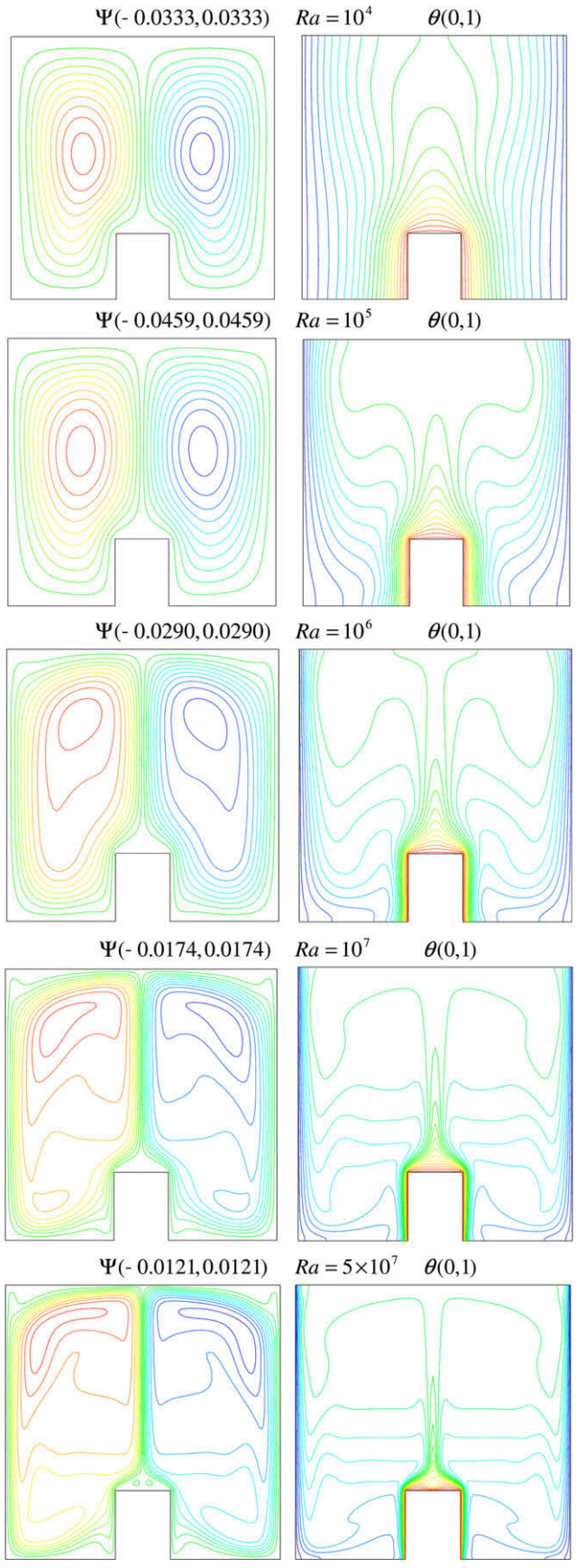

Fig. 4. Effect of varying Rayleigh number on the streamlines and isotherms ($Pr = 0.71$, $W = 0.2$, $D = 0.4$, $H = 0.25$).

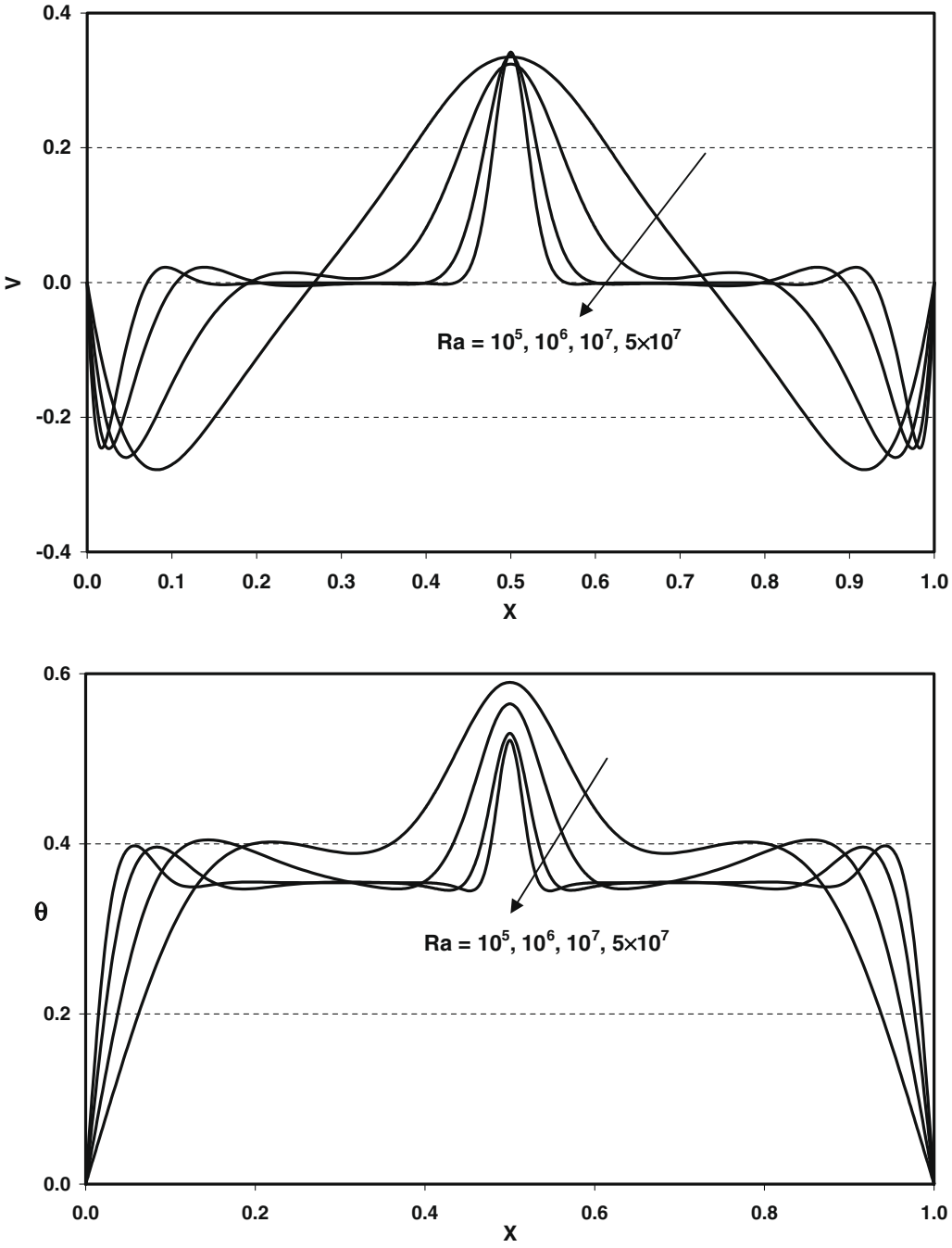

Fig. 5. Effect of Rayleigh number on the *V*-velocity and temperature profiles along a horizontal mid-section of the cavity ($Pr = 0.71$, $W = 0.2$, $D = 0.4$, $H = 0.25$).

physical domain. Moreover, interpolation functions in terms of local normalized element coordinates were implemented to approximate the dependent variables within each element. Subsequently, substitution of the approximations into the system of the governing equations and boundary conditions yielded a residual for each of the conservation equations. These residuals were then reduced to zero in a weighted sense over each element using the Galerkin method.

The highly coupled and non-linear algebraic equations resulting from the discretization of the governing equations were solved using a segregated-solution algorithm. The advantage of this method is that the global system matrix is decomposed into smaller submatrices and then solved in a sequential manner. This technique resulted in considerably fewer storage requirements. A pressure projection algorithm was utilized to obtain a solution for the velocity field at every iteration step. Furthermore, the pressure projection version of the segregated algorithm was used to solve the non-linear system. In addition, the conjugate residual scheme was used to solve the symmetric pressure-type equation systems, while the conjugate gradient squared method was used for the non-symmetric advection-diffusion-type equations.

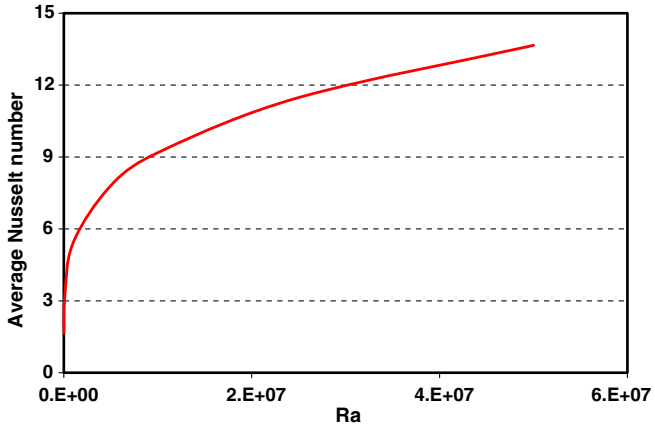

Fig. 6. Effect of Rayleigh number on the average Nusselt number along the left wall of the enclosure ($Pr = 0.71$, $W = 0.2$, $D = 0.4$, $H = 0.25$).

4. Validation

The present numerical code was validated against the benchmark problem of natural convection in a square cavity at various Rayleigh numbers. Table 1 illustrates an excellent comparison of the average Nusselt number between the present results and the numerical results found in the literature [2,19–24]. Figs. 2 and 3 demonstrate a comparison of the isotherms and streamlines between the present results and the results reported by Barakos and Mitsoulis [2] and El-Refaee et al. [23] for various Rayleigh numbers. The comparisons reveal excellent agreement with the reported studies. An additional verification on the accuracy of the present numerical code is displayed in Fig. 4, which demonstrates an excellent comparison of the streamlines between the present numerical results and the PIV-experimental results by Corvaro and Paroncini [16].

5. Results and discussion

The steady-state results presented in this work are generated for different pertinent dimensionless groups: Rayleigh number ($10^4 \leqslant Ra \leqslant 5 \times 10^7$), heater width ($0.005 \leqslant W \leqslant 0.5$), heater height ($0.005 \leqslant H \leqslant 0.5$) and heater location ($0 \leqslant D \leqslant 0.5$). The default parameters are assigned values of $AR = 1$, $W = 0.2$, $D = 0.4$, $H = 0.25$, $Pr = 0.71$ and $Ra = 10^6$ unless otherwise stated. The predicted field variables are presented in terms of the streamlines, isotherms and average Nusselt number.

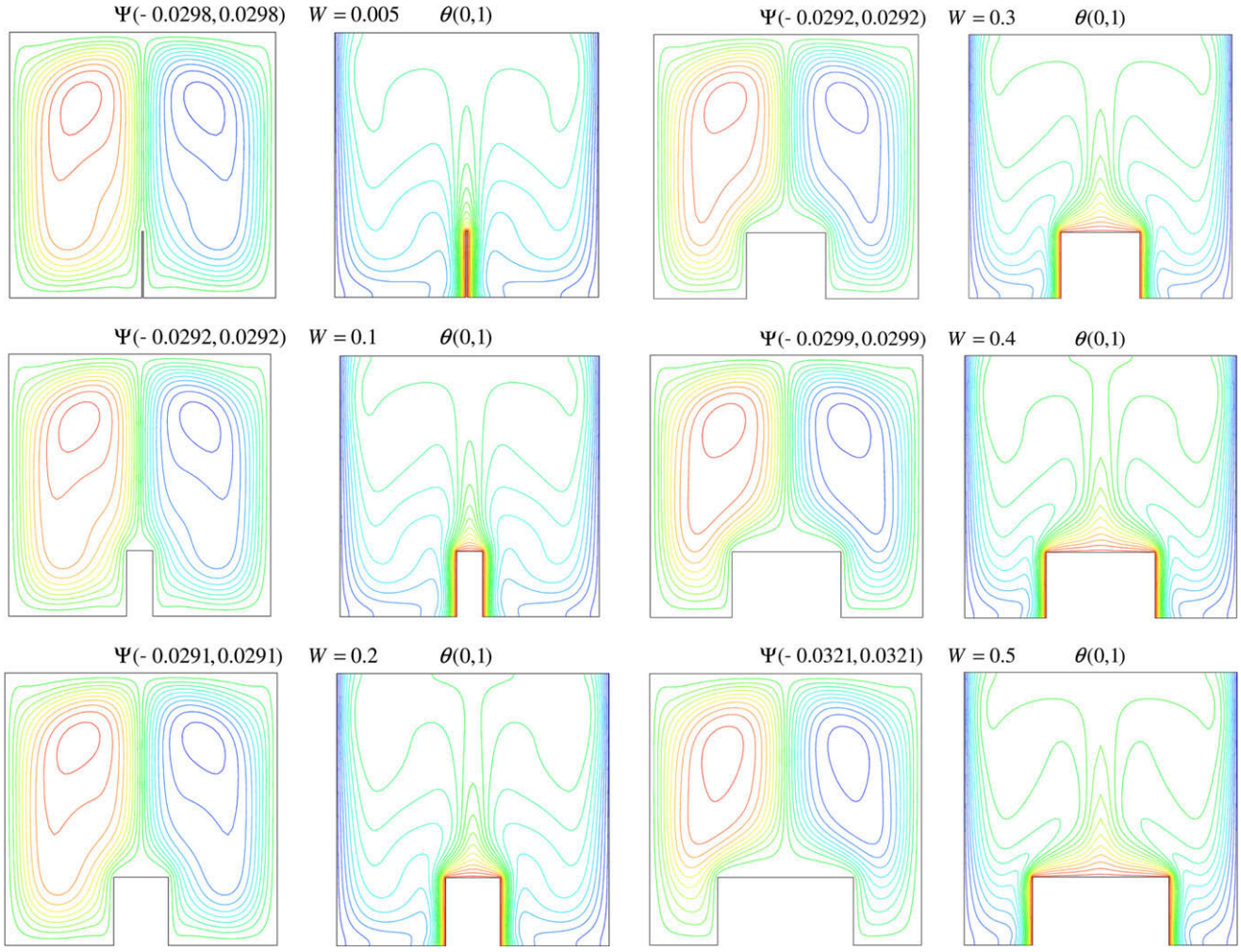

Fig. 7. Effect of varying heater width on the streamlines and isotherms ($Ra = 10^6$, $Pr = 0.71$, $D = 0.4$, $H = 0.25$).

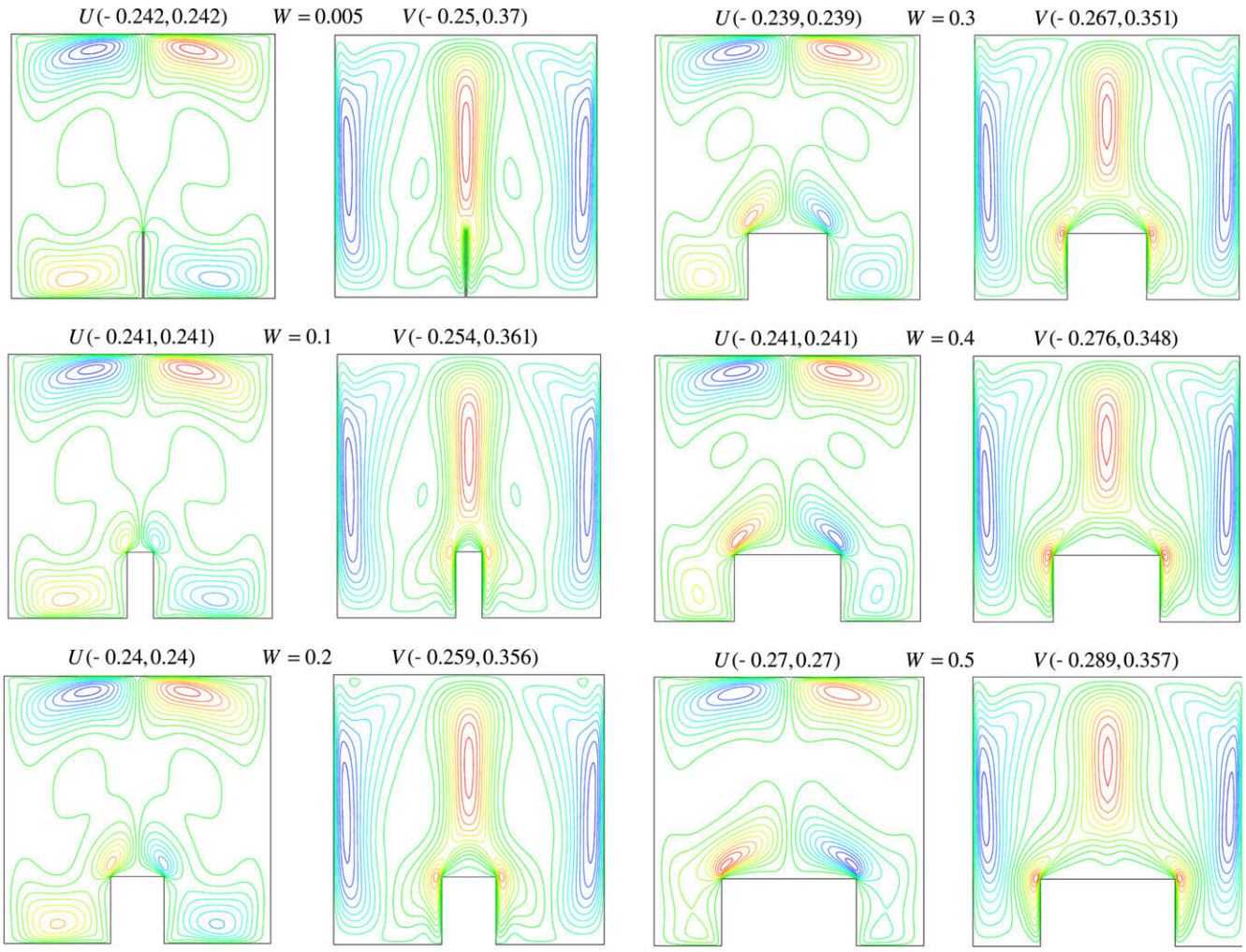

Fig. 8. Effect of varying heater width on the velocity components ($Ra = 10^6$, $Pr = 0.71$, $D = 0.4$, $H = 0.25$).

5.1. Effect of Rayleigh number (Ra)

The effect of Rayleigh number on the streamlines and isotherms is shown in Fig. 4 using $AR = 1$, $W = 0.2$, $D = 0.4$ and $H = 0.25$. For low Rayleigh number values, the streamlines are characterized by two symmetrical counter-rotating vortexes occupying the entire cavity body. The corresponding isotherms are mostly parallel to the vertical walls except along the top surface of the heater. The contribution of convection is noticeable at high Rayleigh numbers as evident by the departure of the isotherms from the vertical pattern. As Rayleigh number increases to $Ra = 10^6$, convection mechanism becomes more pronounced and consequently the central vortex moves upward. Further increase in Rayleigh number to $Ra = 10^7$ causes distortion in the central vortex. In addition, two secondary vortices develop along the bottom surface of the cavity. Fig. 4 shows that the isotherms are horizontal and become vertical inside the very thin boundary layers. This can be attributed to high convection current within the cavity which also causes a reduction in the temperature gradients in the center of the cavity. For even higher values of $Ra = 5 \times 10^7$, Fig. 4 illustrates the presence of two small vortices located on the upper surface of the hot strip. These vortices are generated by the fluid that remains confined inside a small region, created by the two large vortices, on the upper surface of the heater. The velocities at the center of the cavity are very small compared with those at the vertical boundaries as well as above the heater where the fluid is moving fast. This is evident in Fig. 5 where it demonstrates the vertical velocity and temperature profiles along a horizontal plane passing through the center of the cavity. The effect of Rayleigh number on the

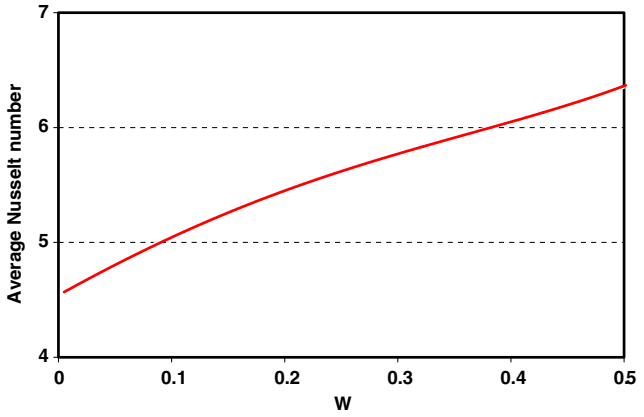

Fig. 9. Effect of the heater width on the average Nusselt number along the left wall of the enclosure ($Ra = 10^6$, $Pr = 0.71$, $D = 0.4$, $H = 0.25$).

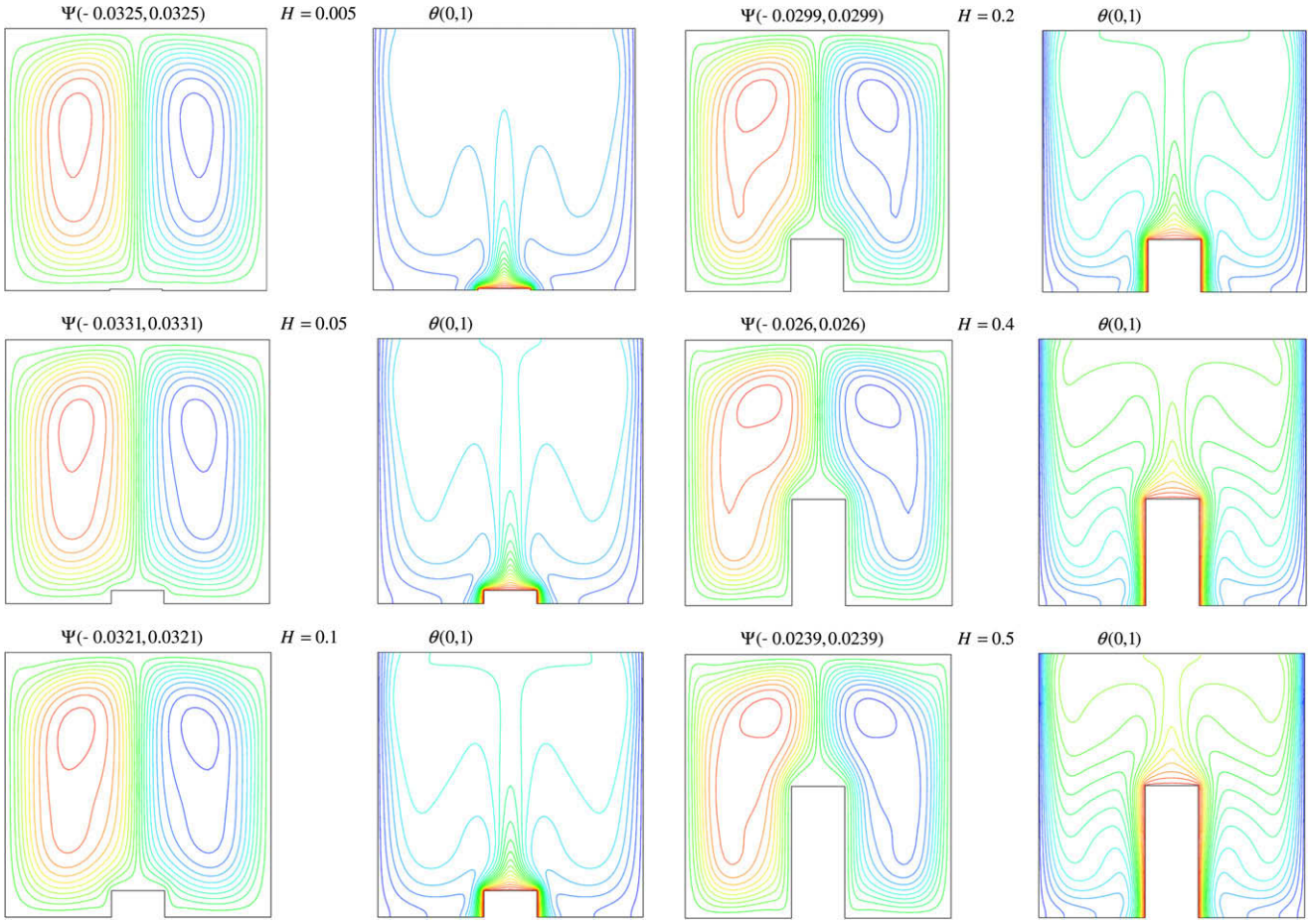

Fig. 10. Effect of varying heater height on the streamlines and isotherms ($Ra = 10^6$, $Pr = 0.71$, $D = 0.4$, $W = 0.2$).

mean Nusselt number of the heater is depicted in Fig. 6. It can be seen from this figure that the average Nusselt number along the left wall of the enclosure increases with increasing Rayleigh number.

5.2. Effect of the heater dimensionless width (W)

The effect of the heater dimensionless width on the streamlines and isotherms is illustrated in Fig. 7. It can be seen from this figure that as the dimensionless width of the heater increases the strength of the circulation is shifted to the left vortex. The left vortex circulates counter-clockwise above the heater since the fluid is heated along the heater and cooled along the cold left wall. However, the right vortex circulates clockwise next to the right wall. The effect of the heater dimensionless width on the isotherms is shown in Fig. 7. A strong plumelike flow is observed with the increasing of the heater width. It is interesting to note from Fig. 7 that the intensity of streamlines decreases as the width of the heater increases from $W = 0.005$ to $W = 0.3$. However, the intensity of streamlines increases for $W \geqslant 0.4$, as depicted in Fig. 7, owing to the thinner boundary layer formation along the vertical walls of the enclosure as the heater approaches the vertical walls. This is evident in Fig. 8 where the vertical velocity component increases significantly along the vertical walls of the enclosure for $W \geqslant 0.4$. The effect of the heater width on the average Nusselt number along the left wall of the enclosure is shown in Fig. 9. As the width of the heater increases, the average Nusselt number enhances due to increasing surface area offered by the heater and increasing intensity of convection current within the enclosure. Although the intensity of convection decreases for heater width ranges between $W = 0.005$ and $W = 0.3$, the average Nusselt number increases since the effect of the heater surface area is dominant.

5.3. Effect of the heater dimensionless height (H)

The effect of the heater dimensionless height on the streamlines and isotherms is demonstrated in Fig. 10. The flow patterns and temperature distributions are symmetrical on either side of the heater as depicted in Fig. 10. As the height of the heater increases, the streamlines values decrease within the enclosure decreases. In addition, the size of the central vortex decreases with increasing the height of the heater. However, Fig. 11 illustrates that the vertical velocity component increases along the vertical walls of the enclosure which indicates thinner boundary layers and, consequently, the overall heat transfer enhances within the enclosure. This is evident in Fig. 12 as the height of the heater increases; the average Nusselt number at the left wall of the enclosure is augmented due to additional surface area offered by the heater for heat transfer communication and thinner boundary layers along the vertical walls of the enclosure.

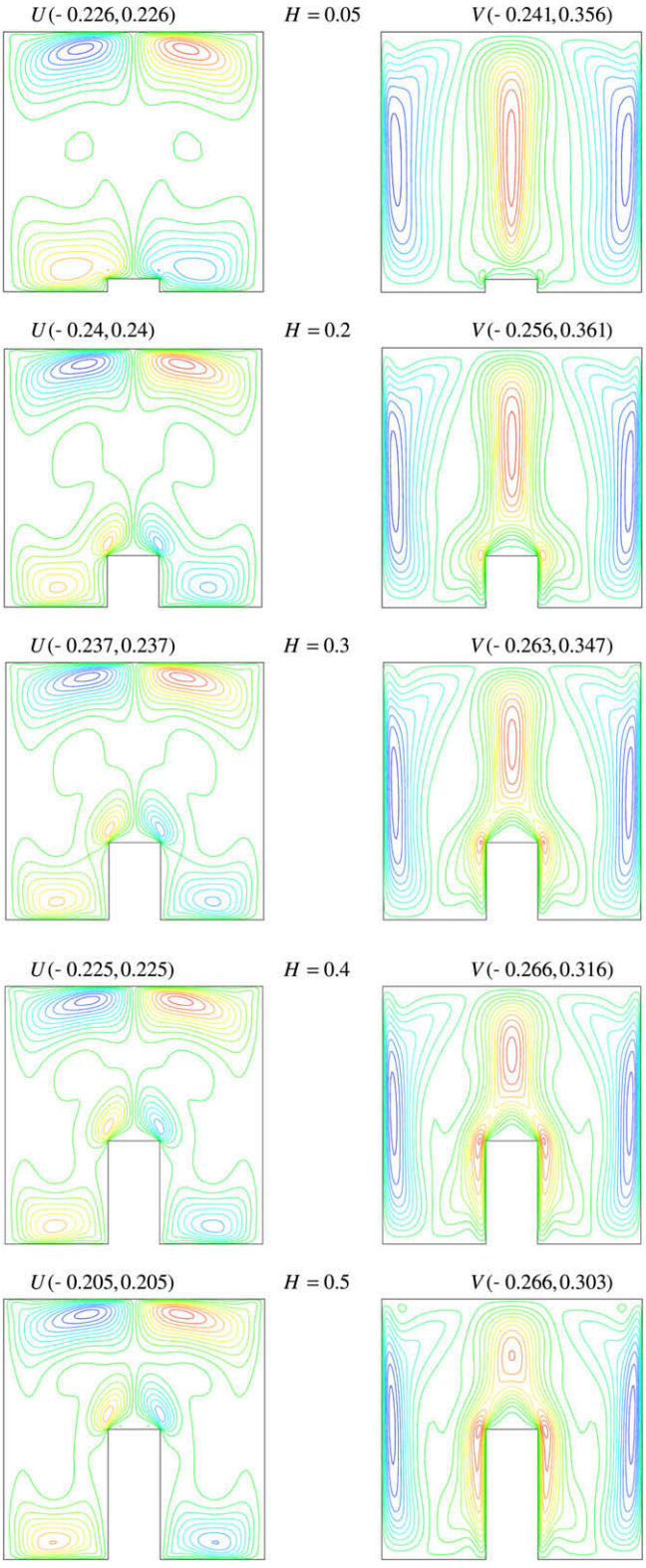

Fig. 11. Effect of varying heater height on the velocity components ($Ra = 10^6$, $Pr = 0.71$, $D = 0.4$, $W = 0.2$).

5.4. Effect of the heater dimensionless location (D)

The effect of the heater dimensionless location on the streamlines and isotherms is illustrated in Fig. 13. As the heater moves towards the center of the enclosure, the strength of the right vortex increases until $D = 0.2$. Afterward, the strength of the right vortex decreases and the strength of the left vortex increases until the heater is symmetrically placed at the middle of the bottom surface i.e., $D = 0.4$. Fig. 14 manifests this observation, where the vertical velocity component along the vertical walls of the enclosure reaches its maximum for $D = 0.2$, and afterwards starts to decrease with an increase in the heater dimensionless location. Fig. 13 shows that further increase in the heater location ($D = 0.5$) causes the flow and temperature patterns to repeat themselves. The effect of the heater location on the average Nusselt number is demonstrated in Fig. 15. As the heater location increases, the average Nusselt number increases significantly until $D = 0.2$ afterward the average Nusselt number increases at a smaller rate.

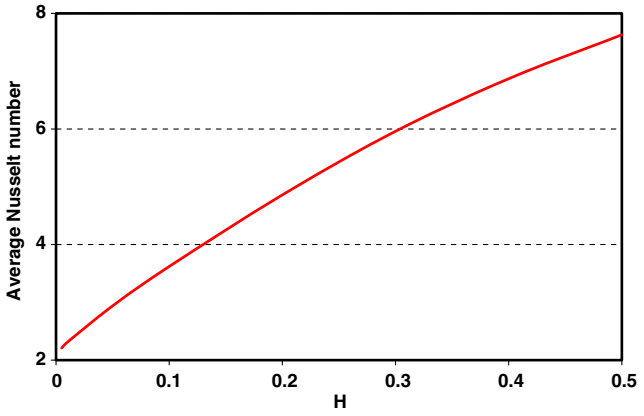

Fig. 12. Effect of the heater height on the average Nusselt number along the left wall of the enclosure ($Ra = 10^6$, $Pr = 0.71$, $D = 0.4$, $W = 0.2$).

6. Heat transfer correlation

The average Nusselt number along the left wall of the enclosure is correlated over a wide range of various pertinent dimensionless groups employed in this investigation, such as the Rayleigh number $10^4 \leqslant Ra \leqslant 5 \times 10^7$, heater thickness ($0.005 \leqslant W \leqslant 0.5$), heater height ($0.005 \leqslant H \leqslant 0.5$) and heater location ($0 \leqslant D \leqslant 0.5$). This correlation can be mathematically expressed as follows:

$$\overline{Nu} = 3.615 + \frac{Ra^{0.441} W^{2.144} H^{2.892} D^{0.429}}{(W+H)^3} \tag{10}$$

where the confidence coefficient for the above equation is $R^2 = 96.6\%$. A graphical representation of the above correlation is illustrated in Fig. 16. This figure demonstrates a very good agreement between the numerical results and those obtained by the correlation.

7. Conclusions

Buoyancy-induced flow and heat transfer in a square cavity with an isothermal protruding heater was studied numerically for various pertinent dimensionless groups. Effects of dimensionless groups representing the Rayleigh number, height of heater, width of the heater and the location of the heater were highlighted to study their impacts on flow structure and heat

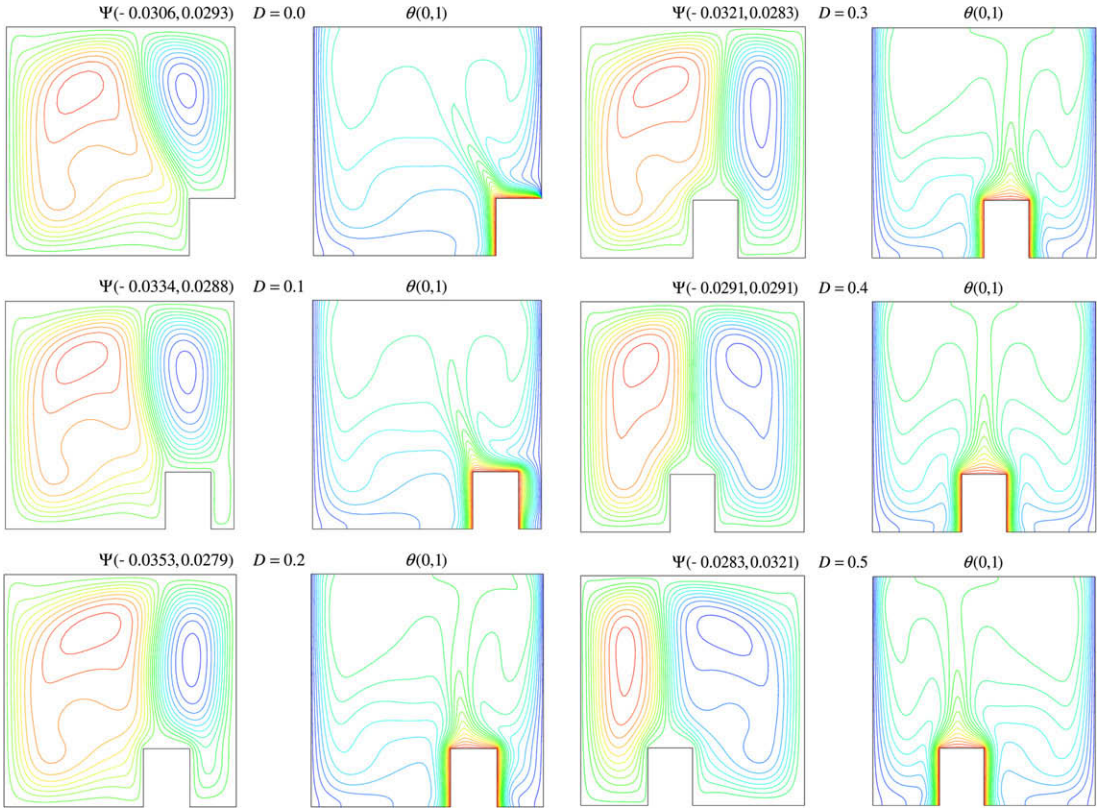

Fig. 13. Effect of varying heater location on the streamlines and isotherms ($Ra = 10^6$, $Pr = 0.71$, $H = 0.25$, $W = 0.2$).

transfer characteristics. The results reveal that Nusselt number increases with the increasing of Rayleigh number. Moreover, it is observed that the location, height and width of the heater have significant effect on flow, temperature fields, and heat transfer. Increased heater height, width and location increase the average Nusselt number.

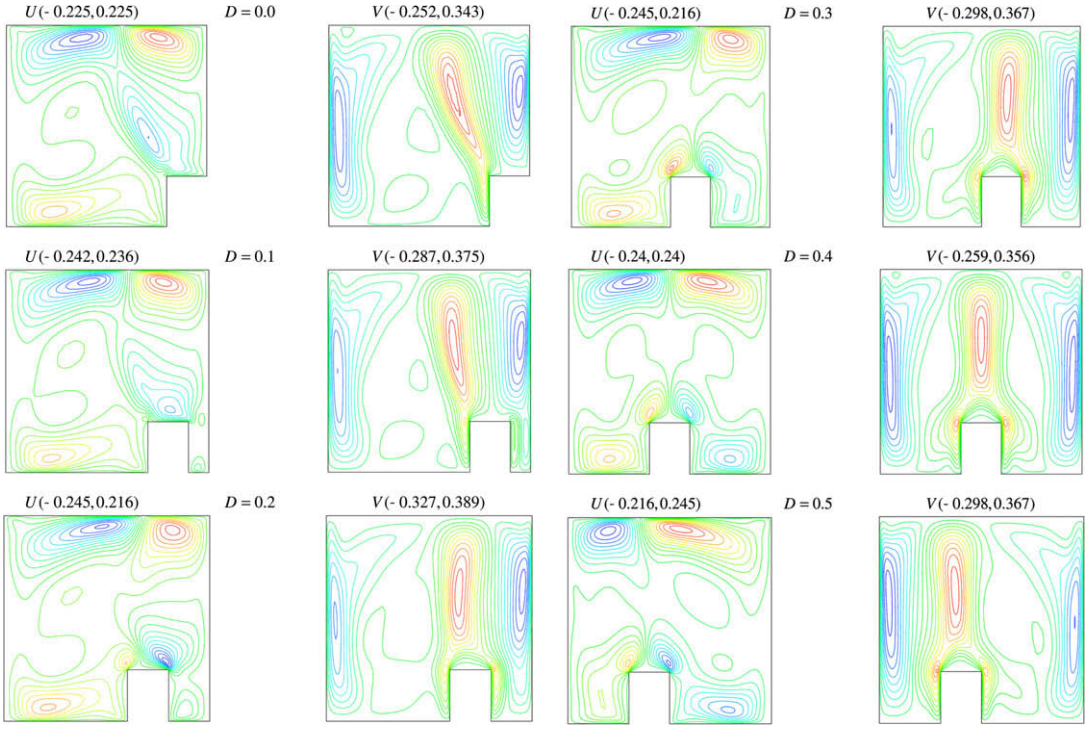

Fig. 14. Effect of varying heater location on the velocity components ($Ra = 10^6$, $Pr = 0.71$, $H = 0.25$, $W = 0.2$).

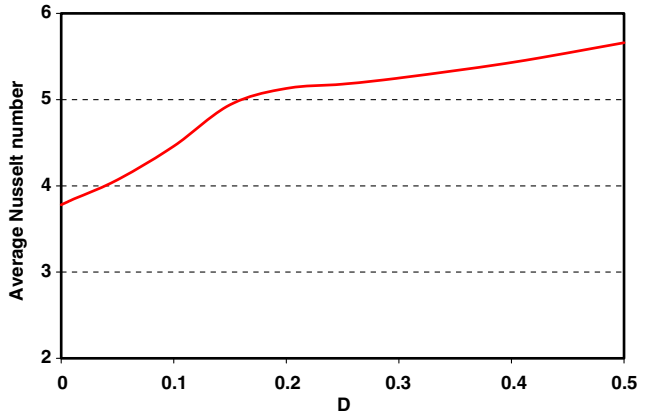

Fig. 15. Effect of the heater location on the average Nusselt number along the left wall of the enclosure ($Ra = 10^6$, $Pr = 0.71$, $H = 0.25$, $W = 0.2$).

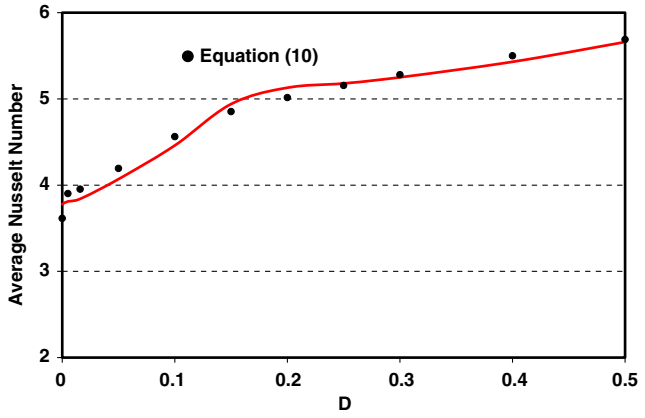

Fig. 16. Comparison of the average Nusselt number between the present numerical results and Eq. (10) ($Ra = 10^6$, $Pr = 0.71$, $H = 0.25$, $W = 0.2$).

References

[1] O.G. Martynenko, P.P. Khramtsov, Free-Convective Heat Transfer: With Many Photographs of Flows and Heat Exchange, Springer, Berlin, 2005.
[2] G. Barakos, E. Mitsoulis, Natural convection flow in a square cavity revisited: laminar and turbulent models with wall functions, Int. J. Numer. Methods Fluids 18 (1994) 695–719.
[3] S. Ostrach, Natural convection in enclosures, ASME J. Heat Transfer 110 (1988) 1175–1190.
[4] M. Afrid, A. Zebib, Natural convection air cooling of heated components mounted on a vertical wall, Numer. Heat Transfer 15 (1989) 243–259.
[5] A. Bar-Cohen, Thermal management of air and liquid-cooled multi-chip modules, IEEE Trans. Components Hybrids Manufacturing Technol. 10 (1987) 159–175.
[6] T.L. Bergman, J.G. Petri, Natural convection cooling of discrete heated elements in an enclosure using pressurized helium-xenon gas mixtures, in: Wirtz, R.A. (Ed.), HTD 100, 1988, pp. 25–33.
[7] H.H.-S. Chu, S.W. Churchill, C.V.S. Patterson, The effect of heater size, location, aspect ratio, and boundary conditions on two- dimensional, laminar, natural convection in rectangular channels, ASME J. Heat Transfer 98 (1976) 194–201.
[8] Z.-G. Du, E. Bilgen, Natural convection in vertical cavities with internal heat generating porous medium, Heat Mass Transfer 27 (1992) 149–155.
[9] R.D. Flack, B.L. Turner, Heat transfer correlations for use in naturally cooled enclosures with high-power integrated circuits, IEEE Trans. Components Hybrids Manufacturing Technol. 3 (1980) 449–452.
[10] K. Khanafer, K. Vafai, Isothermal surface production and regulation for high heat flux applications utilizing porous inserts, Int. J. Heat Mass Transfer 44 (2001) 2933–2947.
[11] Z-D. Due, E. Bilgen, Effects of heat intensity, size, and position of the components on temperature distribution within an electronic PCB enclosure, J. Electron. Packag. 112 (1990) 249–254.
[12] Y. Varol, H.F. Oztop, T. Yilmaz, Natural convection in triangular enclosures with protruding isothermal heater, Int. J. Heat Mass Transfer 50 (2007) 2451–2462.
[13] N. Yucel, A.H. Ozdem, Natural convection in partially divided square enclosure, Heat Mass Transfer 40 (2003) 167–175.
[14] I. Dagtekin, H.F. Oztop, Natural convection heat transfer by heated partitions within enclosure, Int. Comm. Heat Mass Transfer 40 (2001) 823–834.
[15] H. Oztop, E. Bilgen, Natural convection in differentially heated and partially divided square cavities with internal heat generation, Int. J. Heat Fluid Flow 27 (2006) 466–475.
[16] F. Corvaro, M. Paroncini, An experimental study of natural convection in a differentially heated cavity through a 2D-PIV system, Int. J. Heat Mass Transfer 52 (2009) 355–365.
[17] C. Taylor, P. Hood, A numerical solution of the Navier-Stokes equations using finite-element technique, Comput. Fluids 1 (1973) 73–89.
[18] P.M. Gresho, R.L. Lee, R.L. Sani, On the time-dependent solution of the incompressible Navier-Stokes equations in two and three dimensions, in: Recent Adv. Num. Methods in Fluids, Pineridge, Swansea, UK, 1980.
[19] N.C. Markatos, K.A. Pericleous, Laminar and turbulent natural convection in an enclosed cavity, Int. J. Heat Mass Transfer 27 (1984) 772–775.
[20] G. De Vahl Davis, Natural convection of air in a square cavity, a benchmark numerical solution, Int. J. Numer. Methods Fluids 3 (1962) 249–264.
[21] T. Fusegi, J.M. Hyun, K. Kuwahara, B. Farouk, A numerical study of three-dimensional natural convection in a differentially heated cubical enclosure, Int. J. Heat Mass Transfer 34 (1991) 1543–1557.
[22] D.C. Wan, B.S.V. Patnaik, G.W. Wei, A new benchmark quality solution for the buoyancy-driven cavity by discrete singular convolution, Numer. Heat Transfer B 40 (2001) 199–228.
[23] M.M. El-Refaee, M.M. Elsayed, N.M. Al-Najem, I.E. Megahid, Steady-state solutions of buoyancy-assisted internal flows using a fast false, Int. J. Numer. Methods Heat Fluid Flow 6 (1996) 3–23.
[24] R.A.W. Henkes, F.F. Van Der Vlugt, C.J. Hoogendoorn, Natural convection in a square cavity calculated with low-Reynolds-number turbulence model, Int. J. Heat Mass Transfer 34 (1991) 1543–1557.